Determination of Electromagnetic Material Properties of Ferromagnetic Stainless Steel Used in Domestic Induction Heating Cookware

Felix Rehm, Patrick Breining and Marc Hiller

Abstract—Design-oriented modeling approaches, such as finite element analyses (FEA), rely on accurate material data for the modeled hardware. In the case of cookware used in domestic induction heating (IH) systems, manufacturers rarely provide the necessary data. Therefore, this contribution presents results for the electromagnetic material properties of ferromagnetic stainless steel, typically used in cookware for domestic IH. The magnetic material properties are modeled using Jiles-Atherton hysteresis model. With the used measurement method, less effort in preparation of suited material specimen is needed compared to conventional measurement methods. The presented results for the magnetic material properties are validated using Epstein frame measurements. It is shown that the hysteresis curves are similar to each other for both measurement methods. Regarding the specific electrical resistance, the results are validated using a microhmmeter. The values determined for the specific resistance show good accordance for the different measurement methods.

Index Terms—domestic induction heating, load modeling, material characterization, Jiles-Atherton hysteresis model, ferromagnetic stainless steel, cookware

I. INTRODUCTION

Over the past years, domestic induction heating (IH) has become increasingly popular. Regarding its efficiency, cleanliness and the speed of heating the cookware, IH is advantageous compared to classical heating methods such as resistance heating or gas stoves [1].

Fig. 1 shows an exemplary system overview with the main functional parts of a domestic IH system. It consists of an electromagnetic compatibility (EMC) filter, which ensures that grid standards are met for connection to the common voltage grid. Conventional IH systems use a bridge rectifier and a DC-link capacitor with a small capacitance value to ensure a sinusoidal grid current. However, power factor correction (PFC) topologies are used too [2]. The inverter is the main functional part and converts the DC voltage into a mid-frequency (20–150 kHz) AC voltage. A spiral wound induction coil is connected to the output terminals of the

F. Rehm is with the Institute of Electrical Engineering (ETI), Karlsruhe Institute of Technology (KIT), Kaiserstr. 12, 76131 Karlsruhe, Germany (e-mail: felix.rehm@kit.edu)

P. Breining is with the Institute of Electrical Engineering (ETI), Karlsruhe Institute of Technology (KIT), Kaiserstr. 12, 76131 Karlsruhe, Germany (e-mail: patrick.breining@kit.edu)

M. Hiller is with the Institute of Electrical Engineering (ETI), Karlsruhe Institute of Technology (KIT), Kaiserstr. 12, 76131 Karlsruhe, Germany (e-mail: marc.hiller@kit.edu)

inverter and generates a magnetic field, which results in eddy current and hysteresis losses within the bottom of the cookware placed above the coil. The coupled inductor-pot system can be described using different models, which are outlined in the following.

Design-oriented modeling approaches as presented in [3] and [4] make use of linear material properties to calculate frequency-dependent impedance formulas analytically for inductively coupled coils with known geometrical dimensions. Another approach given in [5] makes use of a nonlinear passive network, which consists of frequency-dependent and frequency-independent components. The simplest model is a series connection of an equivalent inductor L_{eq} and an equivalent resistor R_{eq} (see Fig. 2). This can also be described in dependence of the electrical frequency f and the value of the inductor current i_L [6].

Parametrization of the used model can be done through measurements. In [7] a measurement test bench is presented which allows determination of the equivalent impedance of different inductor-pot combinations. Alternatively, finite element analyses (FEA) can be used. FEA require accurate data about geometrical and physical properties of the electromagnetic part of an IH system. The geometrical structure of the cookware bottom can e.g. be determined by using cut samples. As manufacturers of cookware rarely provide detailed information about electromagnetic material properties, special test specimen made of ferromagnetic steel are characterized in [6].

To overcome the need of special test specimen, a novel measurement method to determine the electromagnetic material properties of already manufactured cookware is introduced in [8]. Herein, an analytic model describing the magnetic properties of the ferromagnetic material is used. The analytic description of the magnetization curve does not take hysteresis of the magnetic material into account. Regarding the determination of the specific electrical resistance, this fact leads to a relative error of approximately 16 % between measurements performed with the proposed method and a microhmmeter.

Within the simulation model, different models to describe the electromagnetic material properties can be used. While linear magnetic properties do not consider saturation effects, the model used in [8] does take saturation effects into account while neglecting magnetic hysteresis. Within this work, Jiles-Atherton hysteresis model (JA-Model) will be used. This

Fig. 1. Block diagram of main functional parts of a domestic IH system consisting of grid connection, EMC Filter, rectifier and DC-link, an inverter and the coupled inductor-pot system.
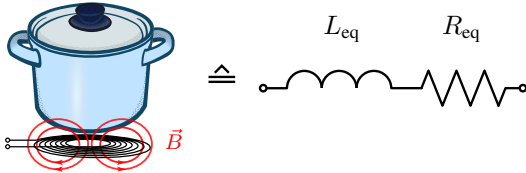
Fig. 2. Equivalent impedance model of the coupled inductor-pot system.

Fig. 3. Schematic of rotational symmetric simulation model with primary coil ①, secondary coil ②, ferrite core ③ and material specimen, which consists of a ferromagnetic bottom layer ④, a nonmagnetic heat transfer layer ⑤ and a ferromagnetic top layer ⑥.

model was firstly introduced in [9] and considers saturation effects as well as magnetic hysteresis.

Following this introduction, Section II describes the measurement method used and the models to describe the electromagnetic material properties. Measurement results are presented in Section III and validated using conventional measurement methods. Section IV gives a conclusion and an outlook on our future work.

II. MEASUREMENT METHOD

According to [8] the measurement method, which is used in the following, is based on minimizing the deviation between measurement and simulation data with respect to parametric defined electromagnetic material properties. A schematic of the magnetic circuit, which exists in hardware and in a simulation model, is shown in Fig. 3. To perform the physical measurements, the magnetic circuit is connected to the output stage of a linear amplifier, which itself is driven by a specific test bench introduced in [10]. The magnetic circuit is a rotational symmetric P-type ferrite core with well-known geometric and physical properties. It serves as the magnetic yoke. Two concentric wound coils are placed within the yoke and are responsible for the excitation of the magnetic circuit (primary coil) and sensing of the flux-linkage through it (secondary coil). The material specimen, which is the multi-layered ferromagnetic cookware bottom to be characterized, is placed on top of the magnetic yoke and closes the magnetic circuit. Due to the rotational symmetric structure of the magnetic circuit, simulations are carried out in terms of two-dimensional (2D) FEA. To be able to set up an exact simulation model, the geometrical structure of the cookware bottom needs to be measured. This can be done with a computed tomography scan or by using cut samples of the material specimen. As depicted in Fig. 4 physical measurements are taken at different operating points of the
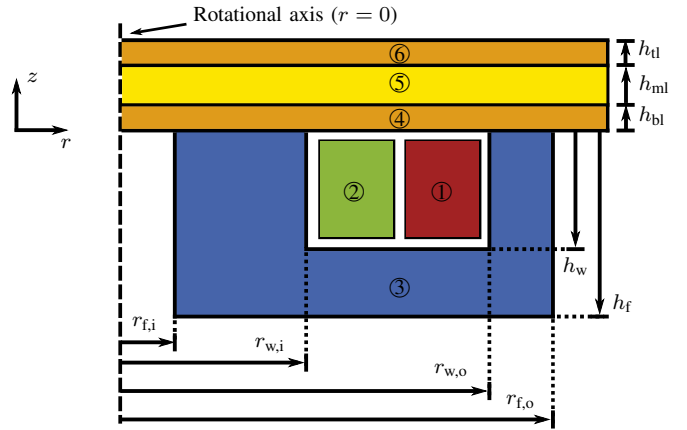
magnetic material, after measuring the layer thicknesses. Measuring different operating points precisely means, the value of the excitation current i_1 varies to reach saturation of the magnetic material within the material specimen. As eddy currents in the pot bottom and therefore the opposing field generated by it, increase with the electrical frequency f of the current through the excitation coil, f is also varied. The recorded excitation current through the primary coil (colored red in Fig. 3) serves as input for the 2D-FEA. The flux-linkage through the magnetic circuit $\Psi_{2,x}$ serves as output of the 2D-FEA and is compared for measurement and simulation data. As shown in Fig. 4 the magnetic material properties are determined at low frequency. Subsequently, the parameters describing the magnetic material properties are taken as constants for the determination of electrical properties at high frequency.

As described in [11], to model magnetic hysteresis, the effective field strength H_e inside a ferromagnetic solid given through

$$H_e = H + \alpha M \tag{1}$$

is used. Therein, H describes the applied magnetic field, M expresses the bulk magnetization and α is a mean field parameter representing interdomain coupling and is simultaneously one parameter of JA-Model. Domain wall
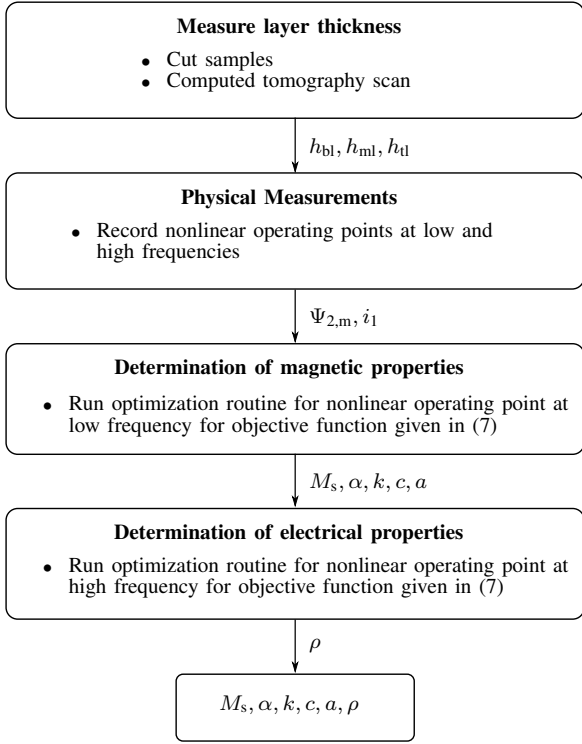
Fig. 4. Resulting workflow of used measurement method with different steps and output variables.

displacement within the ferromagnetic material consists of reversible and irreversible effects [11]. Magnetization M can therefore be expressed as

$$M = M_{\text{irr}} + M_{\text{rev}}, \tag{2}$$

where M_{irr} is the irreversible component and M_{rev} is the reversible component. The irreversible part of (2) is represented as

$$\frac{\mathrm{d}M_{\text{irr}}}{\mathrm{d}H} = \frac{M_{\text{an}} - M_{\text{irr}}}{k\delta/\mu_0 - \alpha(M_{\text{an}} - M_{\text{irr}})}, \tag{3}$$

with δ being $+1$ for $\frac{\mathrm{d}H}{\mathrm{d}t} > 0$ and -1 for $\frac{\mathrm{d}H}{\mathrm{d}t} < 0$, μ_0 the permeability of vacuum and k defining the width of the hysteresis curve. M_{an} describes the anhysteretic or ideal magnetization curve and is given through

$$M_{\text{an}}(H) = M_{\text{s}} \left(\coth \left(\frac{H + \alpha M}{a} \right) - \frac{a}{H + \alpha M} \right), \tag{4}$$

with a defining the shape of the anhysteretic curve and M_{s} being the saturation magnetization. The reversible part of (2) can be described by

$$M_{\text{rev}} = c(M_{\text{an}} - M_{\text{irr}}), \tag{5}$$

with c being another model parameter. Differentiation of (5) and inserting into (2) leads to,

$$\frac{\mathrm{d}M}{\mathrm{d}H} = \frac{1}{(1 + c)} \frac{M_{\text{an}} - M}{k\delta/\mu_0 - \alpha(M_{\text{an}} - M)} + \frac{c}{(1 + c)} \frac{\mathrm{d}M_{\text{an}}}{\mathrm{d}H}. \tag{6}$$

The influence of varying values of the five model parameters M_{s}, α, k, c and a on the shape of the hysteresis curve is given

in detail in [11]. The electrical properties of the cookware bottom layer are modeled through the specific resistance ρ.

To reduce the computational effort during determination of the parameter values, a nonlinear optimization method using interior-point algorithm is used. Herein, the objective function J_{obj} is minimized with respect to the magnetic material parameters M_{s}, α, k, c and a or respectively with respect to the specific resistance ρ. It is defined as

$$J_{\text{obj}} = \sum_{i=1}^{N} (\Psi_{2,\text{m}}(t_i) - \Psi_{2,\text{s}}(t_i))^2, \tag{7}$$

with N being the number of simulated time steps within a period. $\Psi_{2,x}(t_i)$ describes the value of flux-linkage at the time step t_i, with

$$\Psi_{2,x}(t_i) = n_2 \cdot \phi_{2,x}(t_i), \tag{8}$$

while n_2 denotes the number of turns in the secondary coil (colored green in Fig. 3) and $\phi_{2,x}(t_i)$ being the value of the magnetic flux at time step t_i through the magnetic circuit. The values are taken either from measurement ($x \equiv$ m) or simulation data ($x \equiv$ s).

III. EXPERIMENTAL RESULTS

In the following, measurement results will be presented for ferromagnetic stainless steel of type 1.4016 (AISI 430) and the hysteresis curve defined through JA-Model is compared to measurement results generated with an Epstein frame. Measurement results on the Epstein frame are generated for strips of stainless steel under regard of IEC 60404-2. Measurement results on the rotational symmetric ferrite core are generated using the same stainless steel type, which is used for the Epstein frame measurements. The round material specimen has a diameter of $160\,\text{mm}$ and a height h_{bl} of $0.78\,\text{mm}$. Additionally, to emulate the structure of the cookware bottom, a copper layer with height h_{ml} and a second layer of ferromagnetic stainless steel is placed on top of the magnetic yoke according to Fig. 3. The physical and geometrical parameters of the measurement setup are given in Table I.

TABLE I
GEOMETRICAL AND PHYSICAL PARAMETERS OF MEASUREMENT SETUP ACCORDING TO FIG. 3.

Parameter	Value	
Inner ferrite core radius $r_{\text{f,i}}$	4.3	mm
Inner radius winding space $r_{\text{w,i}}$	14.7	mm
Outer radius winding space $r_{\text{w,o}}$	29.2	mm
Outer ferrite core radius $r_{\text{f,o}}$	34.5	mm
Height winding space h_{w}	9.1	mm
Height ferrite core h_{f}	14	mm
Height specimen bottom layer h_{bl}	0.78	mm
Height specimen middle layer h_{ml}	2	mm
Height specimen top layer h_{tl}	0.78	mm
Rel. permeability ferrite core $\mu_{\text{r,ferrite}}$	2300	

A. Determination of magnetic properties

To determine the values of the JA-Model parameters, measurements are taken at an electrical frequency of $f = 10\,\mathrm{Hz}$. The number of turns in the primary and secondary coils are $n_1 = 110$ and $n_2 = 100$, respectively.

The measurement results of the primary current i_1 and the flux-linkage $\Psi_{2,\mathrm{m}}$ (blue curves in Fig. 5a-b) are used as input data for the optimization routine. The flux-linkage $\Psi_{2,\mathrm{s}}$, resulting after minimization of the objective function J_{obj}, is depicted in Fig. 5b. As shown in Fig. 5c, the deviation between measurement and simulation data reaches its maximum at $t = 44\,\mathrm{ms}$. The absolute value of deviation is approximately $0.5\,\mathrm{mWb}$. This equals a relative deviation of $5.38\,\%$ compared to the amplitude of flux-linkage $\Psi_{2,\mathrm{m}}$. Fig. 6 shows the comparison of hysteresis curves determined through Epstein frame measurements and determined through 2D-FEA. Epstein frame measurement and simulation data show a coercive field strength of $H_{\mathrm{c,ef}} = 672\,\mathrm{Am}^{-1}$ and $H_{\mathrm{c,FEA}} = 656\,\mathrm{Am}^{-1}$, respectively. The absolute deviation of $16\,\mathrm{Am}^{-1}$ equals a relative deviation $2.38\,\%$. Regarding the amplitude of polarization at the tip of the hysteresis curve, measurement data from the Epstein frame reaches $J_{\mathrm{max,ep}} = 1.2\,\mathrm{T}$, while FEA data reaches $J_{\mathrm{max,FEA}} = 1.16\,\mathrm{T}$. This corresponds with a relative deviation of $3.33\,\%$. While the deviation for J_{max} and H_{c} is relatively small, the deviation regarding the remanent polarization J_{r} between Epstein frame and FEA data is higher. Herein, $J_{\mathrm{r,ep}} = 0.63\,\mathrm{T}$ and $J_{\mathrm{r,FEA}} = 0.79\,\mathrm{T}$, which equals a relative deviation of $25\,\%$. Nevertheless, Fig. 6 shows that the hysteresis curves measured at Epstein frame and generated using FEA do match for most values of the field strength H. Especially for the ascending part of the hysteresis curves, starting at $+H_{\mathrm{c}}$ into the direction of $+H_{\mathrm{max}}$, both curves are almost identical. In contrast to these results, the deviation regarding the descending part of the hysteresis curves, starting at $+H_{\mathrm{max}}$ into the direction of $-H_{\mathrm{c}}$, is higher. The parameter values given in (6) describing the hysteresis curve using JA-Model are as follows: $M_{\mathrm{s}} = 1\,394\,435\,\mathrm{Am}^{-1}$, $\alpha = 0.003$, $k = 971.46\,\mathrm{Am}^{-1}$, $c = 0.29$ and $a = 1557\,\mathrm{Am}^{-1}$.

B. Determination of electrical properties

To determine the specific electrical resistance ρ of the material specimen, measurements are performed at a frequency of $f = 500\,\mathrm{Hz}$. The number of turns in the primary and secondary coils are $n_1 = 25$ and $n_2 = 20$, respectively. According to the previous results, the magnetic properties are defined as $M_{\mathrm{s}} = 1\,394\,435\,\mathrm{Am}^{-1}$, $\alpha = 0.003$, $k = 971.46\,\mathrm{Am}^{-1}$, $c = 0.29$ and $a = 1557\,\mathrm{Am}^{-1}$ within the FEA. The objective function J_{obj} given in (7) is minimized with respect to ρ. Fig. 7 shows the results of excitation current i_1, the flux-linkages $\Psi_{2,\mathrm{m}}$ and $\Psi_{2,\mathrm{s}}$ as well as the difference between measurement and FEA data. The deviation between measurement and FEA data reaches its maximum at $t = 0.64\,\mathrm{ms}$ with an absolute value of $0.14\,\mathrm{mWb}$. This equals a relative deviation of approximately $9\,\%$ compared to the amplitude of flux-linkage $\Psi_{2,\mathrm{m}}$. The optimization routine reached its stopping

(a) Excitation current i_1

(b) Resulting flux-linkage Ψ_2

(c) Difference between measurement and simulation data $\Psi_{2,\mathrm{m}} - \Psi_{2,\mathrm{s}}$
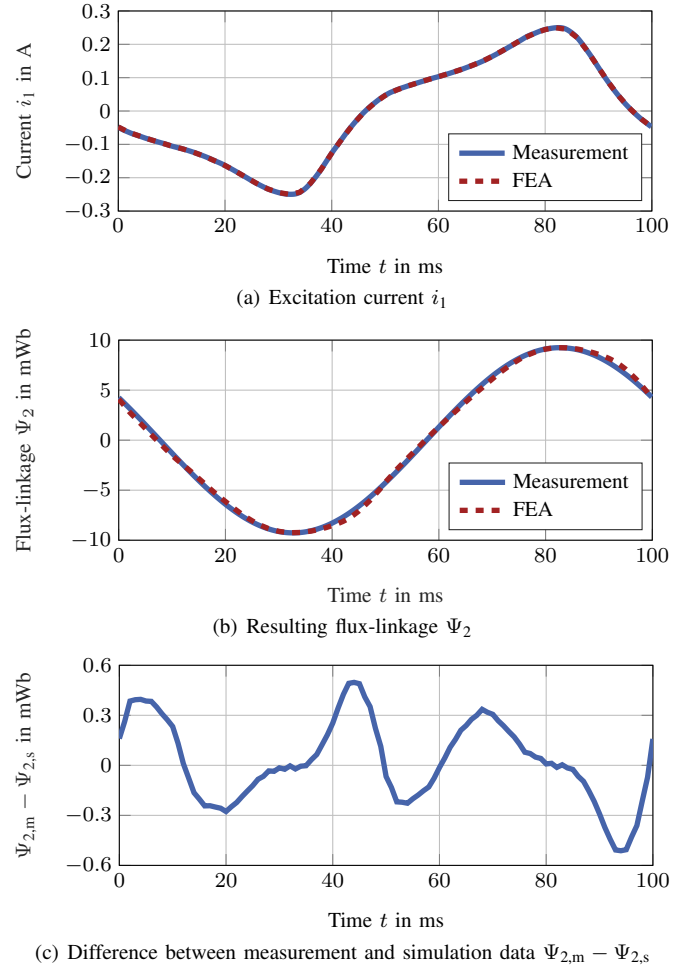
Fig. 5.   (a) Excitation current i_1, (b) resulting flux-linkage $\Psi_{2,\mathrm{m}}$ for measurement (blue curve) and output of optimization routine $\Psi_{2,\mathrm{s}}$ (red curve) as well as (c) difference between measurement and FEA data for flux-linkages $\Psi_{2,\mathrm{m}}$ and $\Psi_{2,\mathrm{s}}$ at $f = 10\,\mathrm{Hz}$.
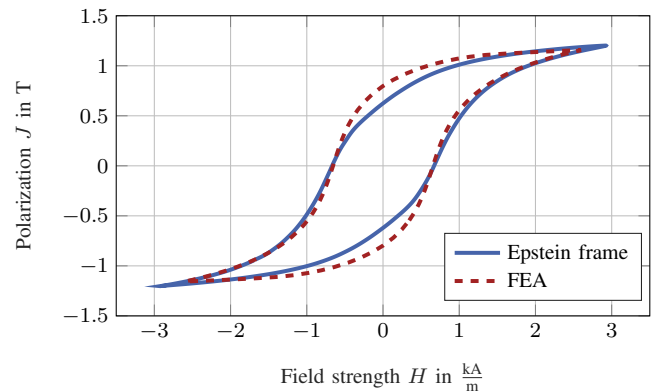
Fig. 6.   Hysteresis curves determined through FEA (red curve) and hysteresis curve measured using an Epstein frame (blue curve).

(a) Excitation current i_1

(b) Resulting flux-linkage Ψ_2

(c) Difference between measurement and simulation data $\Psi_{2,\mathrm{m}} - \Psi_{2,\mathrm{s}}$
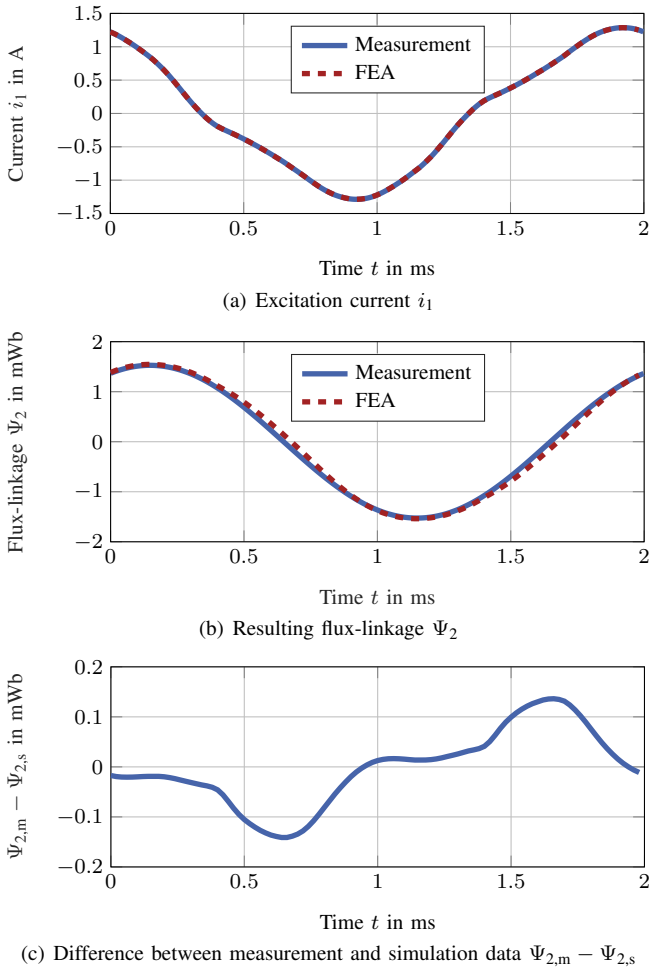
Fig. 7.   (a) Excitation current i_1, (b) resulting flux-linkage $\Psi_{2,\mathrm{m}}$ for measurement (blue curve) and output of optimization routine $\Psi_{2,\mathrm{s}}$ (red curve) as well as (c) difference between measurement and FEA data for flux-linkages $\Psi_{2,\mathrm{m}}$ and $\Psi_{2,\mathrm{s}}$ at $f = 500\,\mathrm{Hz}$.

criterion for a value of $\rho_{\mathrm{FEA}} = 534 \times 10^{-9}\,\Omega\mathrm{m}$. To validate this result, additional resistance measurements are performed using a *"Sefelec MGR10"* microhmmeter and a steel strip of type 1.4016 (AISI 430) with a length $l = 100\,\mathrm{mm}$, a width $w = 30\,\mathrm{mm}$ and a height $h = 0.78\,\mathrm{mm}$. With

$$\rho_{\mathrm{rm}} = R \cdot \frac{w \cdot h}{l} \tag{9}$$

the specific electrical resistance ρ_{rm} can be calculated. For a measured resistance value of $R = 2.42\,\mathrm{m}\Omega$, the specific electrical resistance is given by $\rho_{\mathrm{rm}} = 566.3 \times 10^{-9}\,\Omega\,\mathrm{m}$. The relative deviation between ρ_{FEA} and ρ_{rm} is approximately $5.7\,\%$.

IV. Conclusion and Outlook

In this contribution, we have presented measurement results for determination of the electromagnetic material properties of ferromagnetic stainless steel, which is commonly used in in domestic IH cookware. We made use of a measurement method, which was firstly introduced in [8]. In contrast to [8], in this contribution Jiles-Atherton hysteresis

model is used to model magnetic material properties. Values describing the hysteresis curve are presented and the resulting hysteresis curve is compared to measurement results generated with an Epstein frame. Compared to Epstein frame measurements, less effort is needed in preparation of suited material specimen when using the proposed measurement method. Regarding magnetic hysteresis, the results generated using both methods differ by $16\,\mathrm{Am}^{-1}$ for the coercive field strength H_{c}. For the remanent polarization J_{r} the results for both methods differ by $160\,\mathrm{mT}$. However, the hysteresis curves are similar to each other, especially in the ascending part of the curves for positive values of the field strength H.

Concerning the determination of the specific electrical resistance ρ of the material specimen, the presented results differ by $5.7\,\%$. The value of $\rho_{\mathrm{rm}} = 566.3 \times 10^{-9}\,\Omega\mathrm{m}$ is generated performing resistance measurements using a microhmmeter.

The presented parameter values can be used to describe electromagnetic material properties, for instance for use within FEA during the design process of an IH system. Consequently, the inaccuracy in the modeling of the electromagnetic part of an IH system, introduced by unknown electromagnetic properties of the bottom layer of cookware, is reduced.

Applied to conventional cookware, it should be noted, that the bottom layer often is not exactly flat. This must be taken into account when measuring the geometric structure of the material specimen. To reduce the impact of this rather complex geometry on the measurement results, a possible solution might be to insert an air gap with a known height between the magnetic yoke and the material specimen.

For our future work, we aim to improve the accuracy of the measurement method by using different optimization algorithms and implement temperature-dependent modeling of the specific resistance ρ. Additionally, different types of ferromagnetic stainless steel and different types of cookware will be analyzed.

References

[1] O. Lucia, J. Acero, C. Carretero, and J. M. Burdio, "Induction Heating Appliances: Toward More Flexible Cooking Surfaces," *IEEE Industrial Electronics Magazine*, vol. 7, no. 3, pp. 35–47, Sep. 2013. [Online]. Available: http://ieeexplore.ieee.org/document/6603370/

[2] M. Perez-Tarragona, H. Sarnago, O. Lucia, and J. M. Burdio, "Design and Experimental Analysis of PFC Rectifiers for Domestic Induction Heating Applications," *IEEE Transactions on Power Electronics*, vol. 33, no. 8, pp. 6582–6594, Aug. 2018. [Online]. Available: https://ieeexplore.ieee.org/document/8047988/

[3] W. Hurley and M. Duffy, "Calculation of self and mutual impedances in planar magnetic structures," *IEEE Transactions on Magnetics*, vol. 31, no. 4, pp. 2416–2422, Jul. 1995. [Online]. Available: http://ieeexplore.ieee.org/document/390151/

[4] ——, "Calculation of self- and mutual impedances in planar sandwich inductors," *IEEE Transactions on Magnetics*, vol. 33, no. 3, pp. 2282–2290, May 1997. [Online]. Available: http://ieeexplore.ieee.org/document/573844/

[5] D. Puyal, C. Bernal, J. M. Burdio, I. Millan, and J. Acero, "A new dynamic electrical model of domestic induction heating loads," in *2008 Twenty-Third Annual IEEE Applied Power Electronics Conference and Exposition*.   Austin, TX, USA: IEEE, Feb. 2008, pp. 409–414.

[6] J. Serrano, J. Acero, I. Lope, C. Carretero, J. Burdio, and R. Alonso, "Modeling of domestic induction heating systems with non-linear saturable loads," in *2017 IEEE Applied Power Electronics Conference and Exposition (APEC)*. Tampa, FL, USA: IEEE, Mar. 2017, pp. 3127–3133.

[7] D. Puyal, C. Bernal, J. M. Burdio, J. Acero, and I. Millan, "Methods and procedures for accurate induction heating load measurement and characterization," in *2007 IEEE International Symposium on Industrial Electronics*. Vigo, Spain: IEEE, Jun. 2007, pp. 805–810.

[8] F. Rehm, P. Breining, and M. Hiller, "A measurement method for the characterization of the ferromagnetic bottom layer of cookware used in domestic induction heating," in *IECON 2021 47th Annual Conference of the IEEE Industrial Electronics Society*. Toronto, ON, Canada: IEEE, Oct. 2021, pp. 1–6. [Online]. Available: https://ieeexplore.ieee.org/document/9589834/

[9] D. C. Jiles and D. L. Atherton, "Theory of ferromagnetic hysteresis (invited)," *Journal of Applied Physics*, vol. 55, no. 6, pp. 2115–2120, Mar. 1984. [Online]. Available: http://aip.scitation.org/doi/10.1063/1.333582

[10] M. Veigel, P. Winzer, J. Richter, and M. Doppelbauer, "New FPGA-based and inline-capable measuring method for the identification of magnetic losses in electrical steel," p. 6.

[11] D. C. Jiles, "Theory of ferromagnetic hysteresis," p. 15.

V. Biographies

Felix Rehm was born in Stuttgart, Germany. He received his master's degree in electrical engineering from the Karlsruhe Institute of Technology (KIT) in 2018. Since 2018 he is working as a research associate at the Institute of Electrical Engineering, Elektrotechnisches Institut (ETI), at KIT to receive a Ph.D. degree. His research interests include electromagnetic design and power electronics for domestic induction heating systems.

Patrick Breining was born in Frankenthal, Germany. He received the bachelor's and master's degree in electrical engineering from the Karlsruhe Institute of Technology (KIT) in 2013 and 2015, respectively. He is currently working towards the Ph.D. degree at the Institute of Electrical Engineering, Elektrotechnisches Institut (ETI), at KIT. His research interests include design and control of electrical machines as well as core loss measurements.

Marc Hiller received the Dipl.-Ing. degree in electrical engineering from the Technical University of Darmstadt, Germany in 1999, and the Ph.D. degree in electrical engineering from the University of Federal Armed Forces Munich, Germany in 2008. In 1999, he was with the Traction Converter R&D Department of the Siemens AG in Erlangen, Germany, as an R&D Engineer working on high power drives for freight locomotives. From 1999 to 2004, he was with the Department of Electrical Engineering, University of Federal Armed Forces Munich, as a Ph.D. Student. From 2005 to 2015, he was with Siemens Industry in Nuremberg, Germany, as Project Manager and Head of Power Section Development in the R&D Department for low and medium voltage converters for energy and industrial applications. He is currently with the Karlsruhe Institute of Technology (KIT), Germany, and as Full Professor for power electronic systems and Head of the Institute of Electrical Engineering, Elektrotechnisches Institut (ETI). His current research interests include the areas of design and control of advanced high-power electronics systems and high performance drives. He has authored or coauthored 50+ scientific publications and has filed 25+ patents.
Dr. Hiller was the recipient of the VDE/ETG Best Paper Award in 2005, and in 2009, he was the recipient of the Inventor of the Year of Siemens AG.